Insights into divertor profiles from two-dimensional probe measurements on the TCV tokamak

H. De Oliveira[1], C. Theiler[1], H. Elaian[1] and the TCV team[2]

[1] *Ecole Polytechnique Fédérale de Lausanne (EPFL), Swiss Plasma Center (SPC), CH-1015 Lausanne, Switzerland*

[2] *See author list of S. Coda et al 2019 Nucl. Fusion, accepted*

The Reciprocating Divertor Probe Array (RDPA) is a new diagnostic which provides two-dimensional (2D) Langmuir probe measurements across the TCV divertor plasma up to the X-point, enabling unprecedented insights into divertor profiles. RDPA has been installed in 2018 and tested in the TCV December campaign (15 shots, $\approx 10\ s$ spent in the plasma).

RDPA design

A 2D region is covered in the poloidal plane by combining the fast vertical motion of a linear motor (up to 38 *cm* into the chamber) and a radial array of 12 rooftop Mach probes (1 *cm* radial resolution). The plunge duration is typically 0.35 *s*, the maximum speed can be as high as 2.5 m/s and the maximum acceleration reaches $80 m/s^2$. The diagnostic structure is mounted on the TCV basement floor, as represented in FIG. 1 **a)**. The diagnostic has been built in the limited space (≈ 5 *cm* by ≈ 15 *cm*) between toroidal coils. The gray parts of RDPA shown in FIG. 1 **b)** are graphite heat shields. The white parts are made out of boron nitride, a refractory material with low atomic number ($Z_B = 5$ and $Z_N = 7$). In terms of electronics, the acquisition frequency for both probe voltage and current measurements was 200 kHz in the December 2018 campaign (2 MHz for the upcoming 2019 experiments).

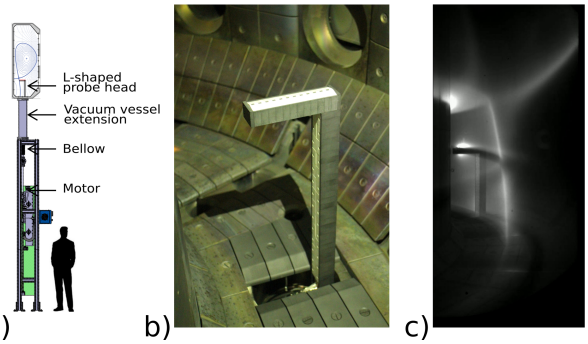

Figure 1: ***a)*** *Poloidal view of RDPA and TCV,* ***b)*** *RDPA during machine opening and* ***c)*** *D4* $\rightarrow$ *2 light snapshot recorded with the MANTIS camera system.*

Deduction of plasma quantities from IV curve measurements

T_e and I_{sat} are obtained by fitting the *IV* curves with a 4 parameters fit [1]. The parallel Mach number is deduced from the ratio of downstream and upstream J_{sat}: $M = \ln(\frac{J_{sat1}}{J_{sat2}})/2.2$. n_e is calculated with a commonly accepted viscous plasma model [2]: $n_e = \frac{J_{sat1}/e}{c_s \exp(-1+1.1M)}$. Finally, the parallel particle flux density is calculated as follows: $\Gamma = v \cdot n_e = M \cdot c_s \cdot n_e = \frac{M J_{sat1}/e}{\exp(-1+1.1M)}$.

Possible perturbations to the plasma and experimental implications

The risk of impurity release from the RDPA surfaces is limited due to a careful material selection choice. Boron nitride cannot be considered as a relevant impurity source due to its low sputtering coefficient. Instead, carbon rich layers have been deposited on the boron nitride surfaces. RPDA affects the local plasma by creating a characteristic dark shadow along the downstream magnetic field lines, as seen on all spectral lines of the MANTIS camera system [4], such as the $D4 \rightarrow 2$ line in FIG. 1 **c)**. The shadow is thought to be caused by the local n_e drop predicted by Mach probes theory. Reducing the diagnostic shadow has been done by minimizing the cross-section of the beam, minimizing f_x and maximizing I_p. For instance, $\approx$ 12% of the Scrape-Off-Layer (SOL) field lines are intercepted by the RPDA beam ($h = 26\ mm$) with $I_p = 320\ kA$ and $f_x = 6$. The bright spots below and above the RDPA beam in FIG. 1 **c)** are believed to be caused by plasma interaction with the neutrals locally generated by surface recombination.

Results in L-Mode plasmas at different plasma densities

The first experiments have been performed in L-Mode with a plasma current of $I_p = 320\ kA$ for different densities, accessing both attached and detached divertor conditions. Edge physics experiment are often performed with density ramps in TCV [3] in order to study the plasma evolution from attached to detached within a single experiment. Since RDPA measurements last $\approx 0.35\ s$, it is not possible to make a steady measurement during a density ramp. Instead multiple shots have been performed with constant densities. The same trend is observed with both methods: the integrated ion flux to the outer target rolls over once $\langle n_e \rangle > 9 \cdot 10^{19} [m^{-3}]$, see FIG. 2.

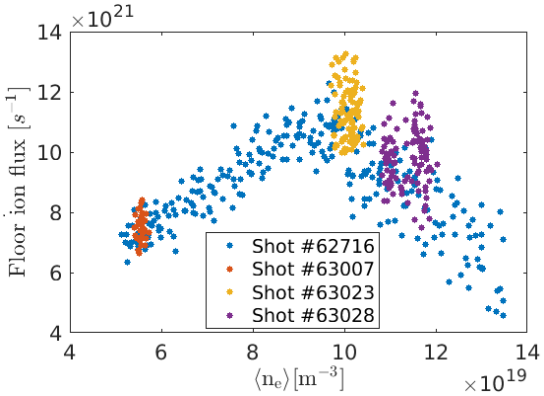

Figure 2: *Integrated outer target ion flux as a function of $\langle n_e \rangle$ obtained from FIR measurements.*

In the discharge #63024 ($\langle n_e \rangle \approx 5.5 \cdot 10^{19} [m^{-3}]$, similar to shot #63007 in FIG. 2), the plasma at the outer target is attached with target T_e exceeding 15 eV. RDPA results are in quantitative agreement with the electron Thomson scattering (TS) measurements near the top of the plunge and with the wall LPs near the target, see FIG. 3. TS T_e values are larger than RDPA values in the near SOL, indicating the presence of a large temperature gradient and an associated conductive heat flux in this region. On the contrary, TS T_e values are very similar to RDPA T_e values in the far SOL, indicating that convective heat flux dominates parallel heat transport in the far SOL.

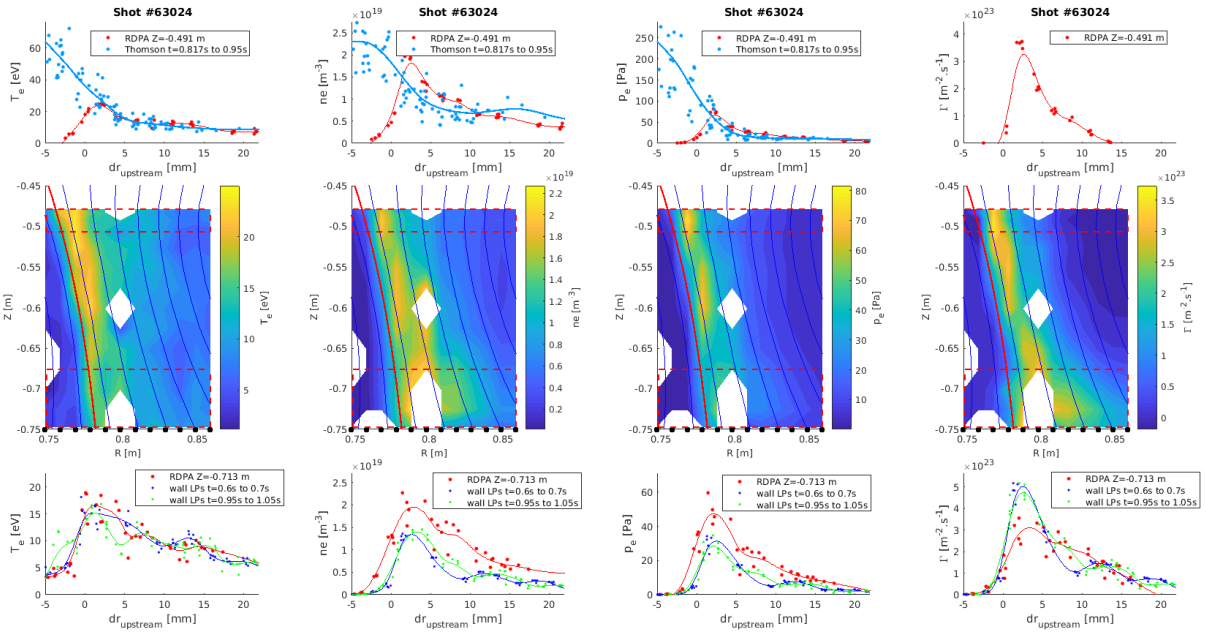

Figure 3: *RDPA, TS and wall LPs profiles of T_e, n_e, p_e and Γ in attached conditions.*

The difference between Γ measurements from wall LPs and from RDPA near the target indicate that ionization within ≈ 1 *cm* from the target could be responsible for $\approx 35\%$ of the peak I_{sat} to the outer target. This could be explained by the recycling process happening locally: the ion target flux results in a flux of wall thermalized D_2 molecules. These rather slow molecules are then susceptible to ionize near the surface with the following route: $D_2 \rightarrow D_2^+ \rightarrow D + D^+$ ($\lambda_{mfp} < 10$ *mm* when $T_e > 10$ *eV*).

In shot #63023 ($\langle n_e \rangle \approx 10 \cdot 10^{19} [m^{-3}]$), the plasma at the outer target is partially detached with target T_e values < 8 *eV*. Here, we enter a regime of higher SOL collisionality, where probe measurements from both RDPA and wall embedded LPs possibly overestimate T_e [1]. A thermal front (steep increase of T_e) is found to develop near the top of the plunge (not shown). This transition region is thought to be correlated with the radiative loss function peak occurring at $T_e \approx 8$ *eV* for carbon impurities in coronal equilibrium [5]. The position of the thermal front matches the position of the *CIII* front given by the MANTIS system. RDPA particle flux measurements indicate that a substantial amount of ionization occurs in the thermal front region. Furthermore, particle flux measurements of RDPA and wall LPs at the target are in excellent agreement and the ionization rate is therefore negligible in the region close to the target.

In shot #63028 ($\langle n_e \rangle \approx 11.5 \cdot 10^{19} m^{-3}$), the plasma at the outer target is partially detached, with electron temperatures < 6 *eV*. In this case, the TS p_e value is higher than the RDPA value, see FIG. 4. Some pressure losses therefore seem to occur above the RDPA plunge region, i.e. in the X-point region. A strong density drop $\Delta n_e \approx 2 \cdot 10^{19} [m^{-3}]$ occurs near the target. This drop would be as high as $\Delta n_e \approx 3.4 \cdot 10^{19} [m^{-3}]$ if we assumed that $T_e = 2$ *eV* instead of the

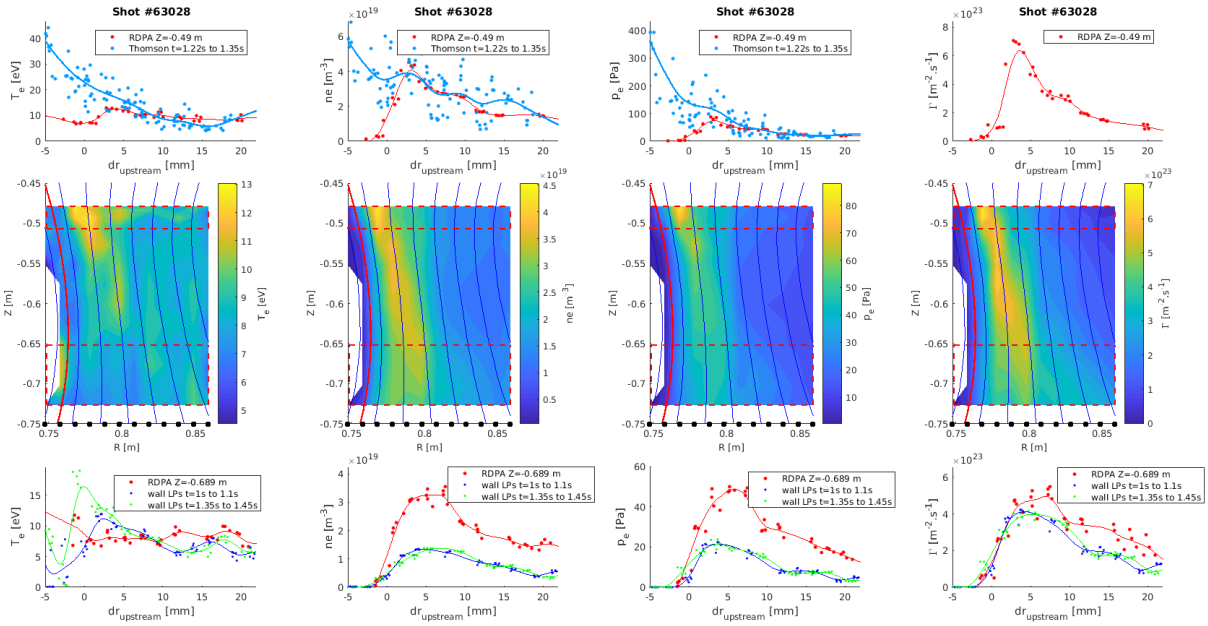

Figure 4: *RDPA, TS and wall LPs profiles of T_e, n_e, n_e and Γ in partially detached conditions.*

LP-inferred values of $T_e \approx 6\ eV$. This corrected value lies in between SOLPS results ($\Delta n_e \approx 1-2\cdot 10^{19}[m^{-3}]$) [6] and divertor spectroscopy measurements ($\Delta n_e \approx 6-7\cdot 10^{19}[m^{-3}]$)[6]. Flow measurements indicate that recombination near the target could be responsible for a $\approx 15\%$ reduction of the peak I_{sat} to the outer target.

Conclusion and outlook

RDPA provide measurements with high spatial and temporal resolution for various plasma quantities across the entire divertor. These measurements agree quantitatively with other reference SOL diagnostics, such as TS and wall LPs. Comparison with simulations will be pursued to better take advantage of the 2D measurements. Some of the diagnostics capabilities have not be presented here and will be the subject of future studies, such as fluctuations measurements (V_{fl}, I_{sat}, M and Γ) and time averaged profiles of V_{pl} and $E\times B$ drifts.

Acknowledgments

This work was supported in part by the Swiss National Science Foundation. This work has been carried out within the framework of the EUROfusion Consortium and has received funding from the Euratom research and training program 2014 - 2018 and 2019 - 2020 under grant agreement No 633053. The views and opinions expressed herein do not necessarily reflect those of the European Commission or of the ITER Organization.

References

[1] O. Février and al., Review of Scientific Instruments **89**, 053502 (2018).
[2] I. H. Hutchinson, Principles of Plasma Diagnostics (Cambridge University Press, 2005).
[3] C. Theiler and al., Nuclear Fusion **57**, 072008 (2017).
[4] A. Perek and al., submitted to Review of Scientific Instruments (2019).
[5] P. C. Stangeby, The Plasma Boundary of Magnetic Fusion Devices (Taylor and Francis, 2000).
[6] K. Verhaegh and al., submitted to Nuclear Fusion (2019).